NeuroImage 133 (2016) 251–265

Contents lists available at ScienceDirect

NeuroImage

journal homepage: www.elsevier.com/locate/ynimg

Estimating repetitive spatiotemporal patterns from resting-state brain activity data

Yusuke Takeda *, Nobuo Hiroe, Okito Yamashita, Masa-aki Sato

Department of Computational Brain Imaging, ATR Neural Information Analysis Laboratories, 2-2-2 Hikaridai, Seika-cho, Soraku-gun, Kyoto 619-0288, Japan

ARTICLE INFO

Article history:
Received 31 July 2015
Accepted 4 March 2016
Available online 12 March 2016

Keywords:
Spatiotemporal pattern
Resting-state
Spontaneous
MEG
EEG
fMRI

ABSTRACT

Repetitive spatiotemporal patterns in spontaneous brain activities have been widely examined in non-human studies. These studies have reported that such patterns reflect past experiences embedded in neural circuits. In human magnetoencephalography (MEG) and electroencephalography (EEG) studies, however, spatiotemporal patterns in resting-state brain activities have not been extensively examined. This is because estimating spatiotemporal patterns from resting-state MEG/EEG data is difficult due to their unknown onsets. Here, we propose a method to estimate repetitive spatiotemporal patterns from resting-state brain activity data, including MEG/EEG. Without the information of onsets, the proposed method can estimate several spatiotemporal patterns, even if they are overlapping. We verified the performance of the method by detailed simulation tests. Furthermore, we examined whether the proposed method could estimate the visual evoked magnetic fields (VEFs) without using stimulus onset information. The proposed method successfully detected the stimulus onsets and estimated the VEFs, implying the applicability of this method to real MEG data. The proposed method was applied to resting-state functional magnetic resonance imaging (fMRI) data and MEG data. The results revealed informative spatiotemporal patterns representing consecutive brain activities that dynamically change with time. Using this method, it is possible to reveal discrete events spontaneously occurring in our brains, such as memory retrieval.

Introduction

Over the past decade, resting-state (or spontaneous) brain activities have attracted much interest, prompting a growing body of neuroscience studies.

In non-human studies, repetitive spatiotemporal patterns emerging in spontaneous brain activities have been widely examined (e.g. Ikegaya et al., 2004). Here, we define spatiotemporal patterns as activities represented by two-dimensional matrices of channel × time (Fig. 1A). These studies have reported that the repetitive spatiotemporal patterns resemble the preceding brain activities during tasks, suggesting that these patterns reflect past experiences embedded in neural circuits (Foster and Wilson, 2006; Han et al., 2008; Ji and Wilson, 2007; Wilson and McNaughton, 1994). Furthermore, it has been reported that the spatiotemporal patterns are predictive of future brain activities during tasks, suggesting that they contribute to the encoding of future novel experiences (Dragoi and Tonegawa, 2011, 2013). Theoretical studies implied that encoding information by spatiotemporal patterns has advantages in terms of the computational efficiency of pattern recognition and memory capacity (Hopfield, 1995; Izhikevich, 2006). All of the above studies highlight the significance of examining spatiotemporal patterns in spontaneous brain activities.

In human studies, functional connectivities of resting-state functional magnetic resonance imaging (fMRI) have been widely examined (Beckmann et al., 2005; Biswal et al., 1995, 2010; Fox et al., 2005; Fox and Raichle, 2007; Raichle et al., 2001; Smith et al., 2009). Functional connectivity is the correlation of fMRI time series across regions, and it is examined using either seed-based correlation (Biswal et al., 2010) or independent component analysis (ICA) (Beckmann et al., 2005). Starting with motor cortices (Biswal et al., 1995), several sets of correlated brain regions were identified, such as the default mode network (DMN) (Fox et al., 2005; Raichle et al., 2001). Recently, Majeed et al. (2011) developed a template-matching algorithm to estimate spatiotemporal patterns from resting-state fMRI data, and they revealed spatiotemporal patterns consisting of an alteration between activation of areas comprising the DMN and the task-positive network.

In human magnetoencephalography (MEG) and electroencephalography (EEG) studies, however, spatiotemporal patterns in resting-state brain activities have not been thoroughly examined. Many of the resting-state MEG/EEG studies also focused on functional connectivity, which here is the correlation of an oscillation's amplitudes across regions. The functional connectivities of MEG/EEG were reported to relate to those of fMRI (Baker et al., 2014; Brookes et al., 2011; de Pasquale et al., 2010, 2012; Mantini et al., 2007). Using clustering methods, some

* Corresponding author. Fax: +81 774 95 1259.
E-mail address: takeda@atr.jp (Y. Takeda).

http://dx.doi.org/10.1016/j.neuroimage.2016.03.014

studies examined spatial patterns in resting-state EEG data, the so-called microstates (Britz et al., 2010; Van de Ville et al., 2010). However, they did not examine the spatiotemporal patterns.

This paucity of research efforts devoted to examining the spatiotemporal patterns in resting-state MEG/EEG data could be attributed to the difficulty of estimating them. In the case of task-related data, spatiotemporal patterns are conventionally estimated using externally observable onsets, such as stimulus and response onsets. For example, the spatiotemporal MEG patterns time-locked at visual stimuli, that is, the so-called visual evoked magnetic fields (VEFs), are obtained by averaging MEG data triggered at the visual stimulus onsets. In the case of resting-state data, however, externally observable onsets do not exist, so the averaging procedure cannot be used. Considering that task-related MEG/EEG data exhibit spatiotemporal patterns time-locked to overt events, it is reasonable to assume that resting-state MEG/EEG data also exhibit spatiotemporal patterns time-locked to covert events, such as memory retrieval (Deuker et al., 2013; Staresina et al., 2013; Tambini et al., 2010).

In the above method of Majeed et al. (2011), a segment starting at a random time point is regarded as a template. Then, segments resembling the template are searched for over time, and the template is updated by averaging the found segments. This method works well when the spatiotemporal patterns do not overlap. If they do overlap, however, the method estimates the spatiotemporal patterns that are contaminated by each other. In the cases of MEG/EEG data, signals from different brain regions are spatially mixed, and thus spatiotemporal patterns probably do overlap. Therefore, their method is not suitable for MEG/EEG data. Because MEG/EEG can capture brain activities on a real electrical time scale, estimating spatiotemporal patterns from these data is also important.

In this study, we propose a method to estimate repetitive spatiotemporal patterns from resting-state brain activity data, including MEG/EEG. Without the information of onsets, the proposed method can estimate several spatiotemporal patterns even if they are overlapping. Using simulated data, we tested the performance of the method in various situations. Furthermore, we tested the performance of this method using real MEG data during a visual stimulation task. We examined whether the proposed method could estimate the VEFs without using stimulus onset information. Finally, the method was applied to resting-state fMRI and MEG data. All of the above analyses confirmed the applicability and usefulness of the proposed method for real brain activity data.

Proposed method to estimate spatiotemporal patterns

Assumption and purpose

Resting-state data are assumed to contain several unknown spatiotemporal patterns at unknown onsets (Fig. 1A), which is expressed as

$$y^{(ch)}(t) = \sum_{k=1}^{K} \sum_{i}^{I_k} p_k^{(ch)}(t - \tau_{k,i} + 1) + v^{(ch)}(t), \tag{1}$$

where $y^{(ch)}(t)$ is resting-state data at channel *ch*, K is the number of spatiotemporal patterns, I_k is the number of onsets for the k-th spatiotemporal pattern, $p_k^{(ch)}(t)$ is the k-th spatiotemporal pattern, $\tau_{k,i}$ is the i-th onset of the k-th spatiotemporal pattern, and $v^{(ch)}(t)$ is noise at channel *ch*. By introducing onset time series

$$u_k(t) = \begin{cases} 1 & t \in [\tau_{k,1}, \cdots, \tau_{k,I_k}] \\ 0 & \text{Otherwise}, \end{cases} \tag{2}$$

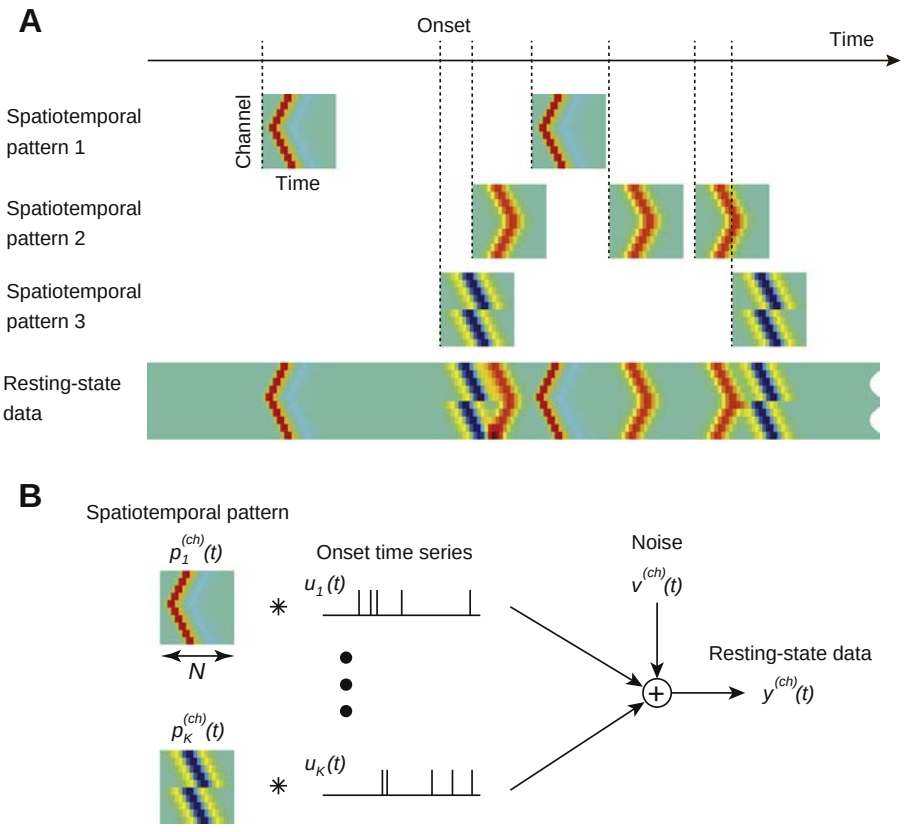

Fig. 1. Assumption of proposed method (STeP). (A): Resting-state data is assumed to contain several unknown spatiotemporal patterns at unknown onsets. Spatiotemporal patterns are defined as activities represented by two-dimensional matrices of channel × time. (B): Schematic representation of Eq. (3). Note that $u_k(t)$ takes a binary (0 or 1) value.

Eq. (1) can be rewritten in a convolution form as

$$y^{(ch)}(t) = \sum_{k=1}^{K}\sum_{n=1}^{N} p_k^{(ch)}(n)u_k(t-n+1) + v^{(ch)}(t), \quad (3)$$

where N is the length of spatiotemporal patterns (Fig. 1B). Eq. (3) can be regarded as the finite impulse response (FIR) model, where $\boldsymbol{p} = \{p_k^{(ch)}(t) | k = 1:K, ch = 1:CH, t = 1:N\}$ and $\boldsymbol{u} = \{u_k(t) | k = 1:K, t = 1:T\}$ correspond to the impulse response and the input, respectively. In the following, the notation $x = 1:X$ is used to represent $x = 1, \cdots, X$. Note that $\boldsymbol{u}$ takes a binary (0 or 1) value and is unknown in this study. Furthermore, the waveforms of $\boldsymbol{p}$ can be different across channels and are also unknown.

The purpose of the proposed method is to estimate $\boldsymbol{p}$ and $\boldsymbol{u}$ from $\boldsymbol{y} = \{y^{(ch)}(t) | ch = 1:CH, t = 1:T\}$, given K and N. Hereafter, this method is called STeP (SpatioTemporal Pattern estimation).

Objective function

STeP attempts to estimate $\boldsymbol{p}$ and $\boldsymbol{u}$ so that the power of the residual error between observed and reconstructed data by the estimated $\boldsymbol{p}$ and $\boldsymbol{u}$ becomes small. Therefore, the objective function is defined as

$$R(\boldsymbol{p}, \boldsymbol{u}) = \sum_{ch=1}^{CH}\sum_{t=1}^{T}\left[y^{(ch)}(t) - \sum_{k=1}^{K}\sum_{n=1}^{N} p_k^{(ch)}(n)u_k(t-n+1)\right]^2. \quad (4)$$

STeP searches for the optimal $\boldsymbol{p}$ and $\boldsymbol{u}$ that minimize $R(\boldsymbol{p}, \boldsymbol{u})$.

Optimization algorithm

If $\boldsymbol{u}$ is given, $\boldsymbol{p}$ can be estimated by the least squares method. On the other hand, if $\boldsymbol{p}$ is given, we can search for $\boldsymbol{u}$. Therefore, from an initial $\boldsymbol{u}$, we can obtain an estimate of $\boldsymbol{u}$ by alternately iterating the updates of $\boldsymbol{p}$ and $\boldsymbol{u}$. However, the converged $\boldsymbol{u}$ may be a local minimum of the objective function [Eq. (4)]. To avoid local minima, we need to repeat this procedure from various initial values of $\boldsymbol{u}$. Furthermore, to generate the initial $\boldsymbol{u}$, we need to set the number of onsets, but this is unknown. To deal with these issues, we developed an optimization algorithm consisting of three hierarchical levels: top, middle, and bottom (Fig. 2A). The top level is for estimating the necessary number of onsets. The middle level is for avoiding local minima by generating various initial values of $\boldsymbol{u}$. The bottom level is for actually estimating $\boldsymbol{u}$. These three levels are described below.

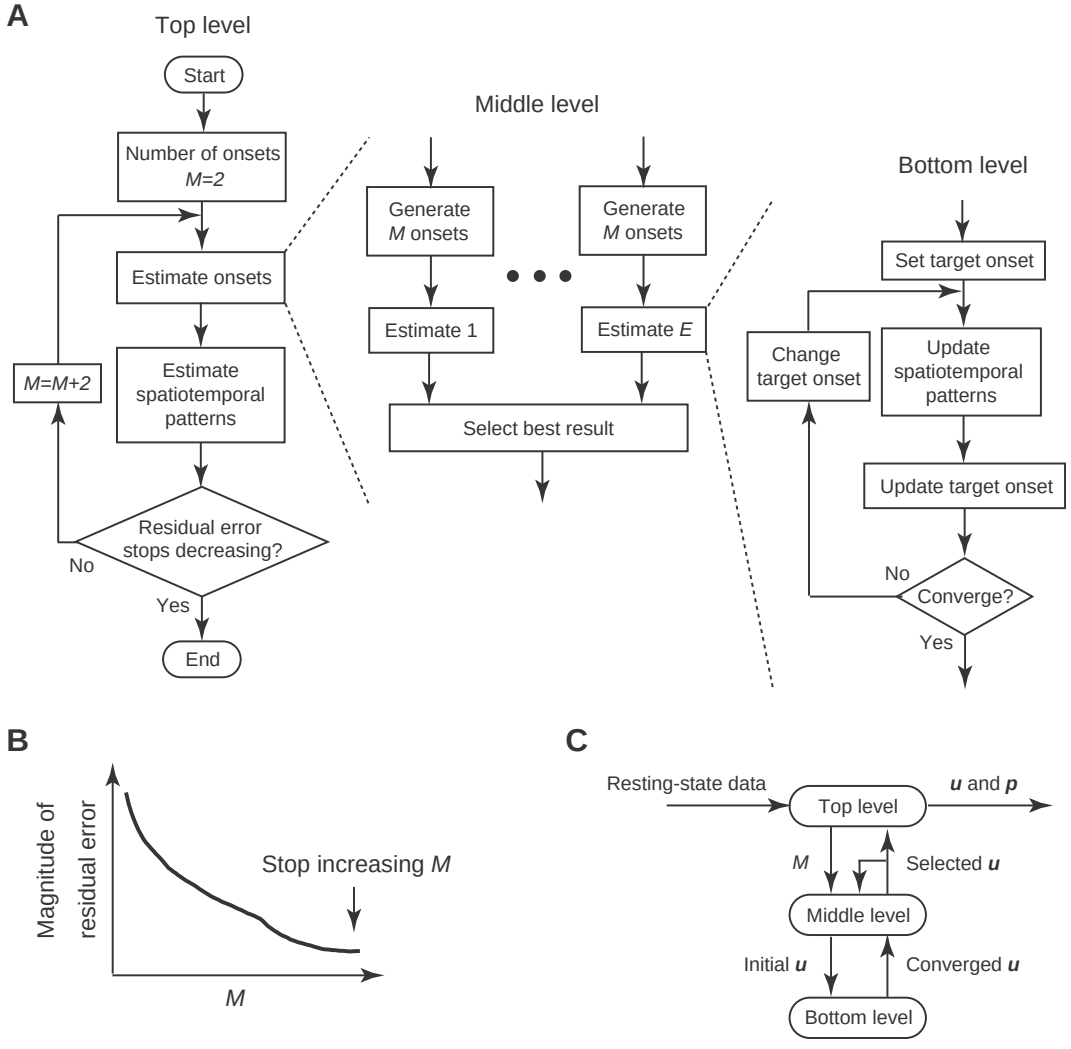

Fig. 2. Algorithm of proposed method (STeP). (A): Flowchart to estimate spatiotemporal patterns and their onsets. At top level, onsets and spatiotemporal patterns are estimated while gradually increasing the number of onsets M. At middle level, given M, estimation of onsets is repeated for E times using different initial onsets, and the best onsets are selected. At bottom level, onsets are estimated from given initial onsets. (B): Schematic representation of top level. As M increases, magnitude of residual error becomes smaller until M reaches a sufficient value. (C): Information flow across the top, middle, and bottom levels.

Top level

This level is for estimating the necessary number of onsets. We first set the number of onsets for each spatiotemporal pattern to M. Because some of the M onsets generated at the middle level can be removed at the bottom level (see middle and bottom levels), M defines the upper limit of the number of onsets for each spatiotemporal pattern. We set common M across k. Then, we estimate $\boldsymbol{u}$ (see middle and bottom levels). Once $\boldsymbol{u}$ is obtained, $\boldsymbol{p}$ can be estimated by the least squares method as follows. Eq. (3) is rewritten in a matrix form as

$$\boldsymbol{Y} = \boldsymbol{U}\boldsymbol{P} + \boldsymbol{V},$$

where

$$\boldsymbol{Y} = \begin{bmatrix} y^{(1)}(T) & \cdots & y^{(CH)}(T) \\ y^{(1)}(T-1) & \cdots & y^{(CH)}(T-1) \\ \vdots & \cdots & \vdots \\ y^{(1)}(N) & \cdots & y^{(CH)}(N) \end{bmatrix},$$

$$\boldsymbol{U} = \begin{bmatrix} u_1(T) & \cdots & u_1(T-N+1) & \cdots & u_K(T) & \cdots & u_K(T-N+1) \\ u_1(T-1) & \cdots & u_1(T-N) & \cdots & u_K(T-1) & \cdots & u_K(T-N) \\ \vdots & \cdots & \vdots & \cdots & \vdots & \cdots & \vdots \\ u_1(N) & \cdots & u_1(1) & \cdots & u_K(N) & \cdots & u_K(1) \end{bmatrix},$$

$$\boldsymbol{P} = \begin{bmatrix} p_1^{(1)}(1) & \cdots & p_1^{(CH)}(1) \\ \vdots & \cdots & \vdots \\ p_1^{(1)}(N) & \cdots & p_1^{(CH)}(N) \\ \vdots & \cdots & \vdots \\ p_K^{(1)}(1) & \cdots & p_K^{(CH)}(1) \\ \vdots & \cdots & \vdots \\ p_K^{(1)}(N) & \cdots & p_K^{(CH)}(N) \end{bmatrix},$$

$$\boldsymbol{V} = \begin{bmatrix} v^{(1)}(T) & \cdots & v^{(CH)}(T) \\ v^{(1)}(T-1) & \cdots & v^{(CH)}(T-1) \\ \vdots & \cdots & \vdots \\ v^{(1)}(N) & \cdots & v^{(CH)}(N) \end{bmatrix}.$$

The least squares solution of $\boldsymbol{P}$ is

$$\hat{\boldsymbol{P}} = \left[\boldsymbol{U}^T\boldsymbol{U}\right]^{-1}\boldsymbol{U}^T\boldsymbol{Y}. \tag{5}$$

Finally, we calculate $R(\boldsymbol{p},\boldsymbol{u})$.

As M increases, $R(\boldsymbol{p},\boldsymbol{u})$ becomes smaller until M reaches a sufficient value (Fig. 2B). Therefore, we gradually increase M until $R(\boldsymbol{p},\boldsymbol{u})$ stops decreasing. In this study, we increased M from 2 by 2 and then stopped increasing it if $R(\boldsymbol{p},\boldsymbol{u})$ did not exceed its minimum value in three consecutive loops, or when M reached T/N.

Middle level

At this level, given M, we try to find the global minimum solution of $\boldsymbol{u}$. Because $R(\boldsymbol{p},\boldsymbol{u})$ has local minima, the initial $\boldsymbol{u}$ does not need to converge to the global minimum. To find the global minimum, we repeat the estimation of $\boldsymbol{u}$ (see bottom level) for E times from different initial $\boldsymbol{u}$ values and select the best $\boldsymbol{u}$ that minimizes $R(\boldsymbol{p},\boldsymbol{u})$, where $\boldsymbol{p}$ is obtained using $\boldsymbol{u}$ by Eq. (5). E was set to 30 in this study. The selected $\boldsymbol{u}$ is preserved for use in generating the initial $\boldsymbol{u}$ next time (i.e. when $M = M+2$).

When $M=2$, the initial $\boldsymbol{u}$ is generated by using only random numbers. Otherwise, it is generated using the preserved $\boldsymbol{u}$ and random numbers. Suppose that the current and last M are m and $m-2$, respectively. We generated the m initial onsets for each spatiotemporal pattern by adding onsets generated by random numbers to the onsets estimated when $M=m-2$. For example, if 5 onsets are estimated for a spatiotemporal pattern when $M=6$, now ($M=8$) we generate 8 onsets by adding 3 onsets to the 5 onsets. Such randomness is introduced only at this level for adding the onsets.

Bottom level

At this level, we actually estimate $\boldsymbol{u}$ from the initial $\boldsymbol{u}$. Namely, onsets $\boldsymbol{\tau} = \{\tau_{k,i} | k = 1:K, i = 1:I_k\}$ are estimated by sequentially updating each onset one by one. Once $\boldsymbol{\tau}$ is estimated, $\boldsymbol{u}$ can be determined according to Eq. (2). Let $\tau_{\tilde{k},\tilde{i}}$ denote the target onset to be updated. We iterate

p-step Update spatiotemporal patterns using onsets except for the target onset $\tau_{\tilde{k},\tilde{i}}$

u-step Update the target onset $\tau_{\tilde{k},\tilde{i}}$ so that the residual error becomes smaller

while changing the target onset with the following order: $\tilde{k} = 1:K$, $\tilde{i} = 1:I_K$. The two steps are described below.

At **p-step**, onset time series not containing the target onset $\tau_{\tilde{k},\tilde{i}}$ are generated by

$$u'_k(t) = \begin{cases} 0 & t = \tau_{\tilde{k},\tilde{i}} \\ u_k(t) & \text{Otherwise.} \end{cases}$$

Using $\boldsymbol{u}' = \{u'_k(t) | k = 1:K, t = 1:T\}$, $\boldsymbol{p}' = \{p'^{(ch)}_k(t) | k = 1:K, ch = 1:CH, t = 1:N\}$ is obtained by Eq. (5).

At **u-step**, a residual error is calculated by

$$r^{(ch)}(t) = y^{(ch)}(t) - \sum_{k=1}^{K}\sum_{n=1}^{N} p'_k{}^{(ch)}(n)u'_k(t-n+1).$$

Because $\boldsymbol{u}'$ does not assume the target onset $\tau_{\tilde{k},\tilde{i}}$, the $\tilde{k}$-th spatiotemporal pattern $p'^{(ch)}_{\tilde{k}}(t)$ is expected to remain in $r^{(ch)}(t)$ around $\tau_{\tilde{k},\tilde{i}}$. Therefore, a candidate time point for the target onset is obtained by

$$t_{new} = \underset{t_0 \in \boldsymbol{t}}{\operatorname{argmin}} \sum_{ch=1}^{CH}\sum_{t=1}^{T} \left[r^{(ch)}(t) - p'^{(ch)}_{\tilde{k}}(t - t_0 + 1)\right]^2,$$

where $\boldsymbol{t}$ is the set of time points between the previous and next onsets of the target onset $[\tau_{\tilde{k},\tilde{i}-1}+1, \cdots, \tau_{\tilde{k},\tilde{i}+1}-1]$. The target onset is updated to t_{new} only if

$$\sum_{ch=1}^{CH}\sum_{t=1}^{T} \left[r^{(ch)}(t) - p'_{\tilde{k}}{}^{(ch)}(t - t_{new} + 1)\right]^2 < \sum_{ch=1}^{CH}\sum_{t=1}^{T} r^{(ch)}(t)^2.$$

Otherwise, the target onset is removed by assuming the onset is not necessary within $\boldsymbol{t}$. Therefore, the number of estimated onsets can be smaller than M and different across k.

The decision of convergence is conducted once in updating all of the onsets. We estimate $\boldsymbol{p}$ using all onsets by Eq. (5) and then calculate $R(\boldsymbol{p},\boldsymbol{u})$. We exit the loop if $R(\boldsymbol{p},\boldsymbol{u})$ is not smaller than that at the previous decision.

Different spatiotemporal patterns are automatically assigned to different k in estimating $\boldsymbol{u}$ at the middle and bottom levels. This is because assigning different spatiotemporal patterns to different k minimizes $R(\boldsymbol{p},\boldsymbol{u})$ more than the other approaches, such as assigning the same spatiotemporal pattern to different k.

Fig. 2C illustrates the information flow across the top, middle, and bottom levels. At the top level, we set M and pass it to the middle level. At the middle level, given M, we generate the initial $\boldsymbol{u}$ and pass it to the bottom level. At the bottom level, from the initial $\boldsymbol{u}$, we estimate $\boldsymbol{u}$ and return it to the middle level. These steps are repeated for E times with different initial $\boldsymbol{u}$, and as a result E-estimated $\boldsymbol{u}$ are obtained. At the middle level, from the E-estimated $\boldsymbol{u}$, we select the best $\boldsymbol{u}$ and return it to the top level. Furthermore, we preserve it for generating the initial $\boldsymbol{u}$ when $M = M+2$.

Materials and methods

Simulation test

The performances of STeP were examined using simulated MEG/EEG data.

Simulated data were generated as follows. Spatiotemporal patterns were generated while setting the number of channels to 10 (Fig. 3A, left). The lengths of the spatiotemporal patterns and simulated data were respectively set to 20 and 6000, corresponding to 0.4 and 120 s when the sampling rate in an offline analysis is 50 Hz. We generated 150 onsets for each spatiotemporal pattern using random numbers. From the onsets, the onset time series were generated according to Eq. (2) (Fig. 3A, right). By summing the convolutions of the spatiotemporal patterns and their onset time series, we obtained a signal time series (Fig. 3B). Simulated data were generated by adding Gaussian white noise to the signal time series (Fig. 3C). The standard deviation (SD) of the noise was either 0.22, 0.40, or 0.71 corresponding to the SNRs of 0, −5, and −10, respectively. The SNR is defined as

$$10\log_{10}\frac{T\sum_{ch=1}^{CH}\sum_{t=1}^{N}p_k^{(ch)}(t)^2}{N\sum_{ch=1}^{CH}\sum_{t=1}^{T}v^{(ch)}(t)^2},$$

where $\sum_{ch=1}^{CH}\sum_{t=1}^{N}p_k^{(ch)}(t)^2$ is the same across k. By applying STeP to the simulated data, we estimated the spatiotemporal patterns and their onsets.

Before quantifying the estimation accuracy, it was necessary to change the assignment of estimated spatiotemporal patterns to k. This is because different spatiotemporal patterns are arbitrarily assigned to different k in the estimation. Furthermore, it was also necessary to adjust the average of the estimated onsets for each spatiotemporal pattern. This is because the shape of a spatiotemporal pattern shifts forward or backward depending on the definition of its onsets, and these are also arbitrarily determined in the

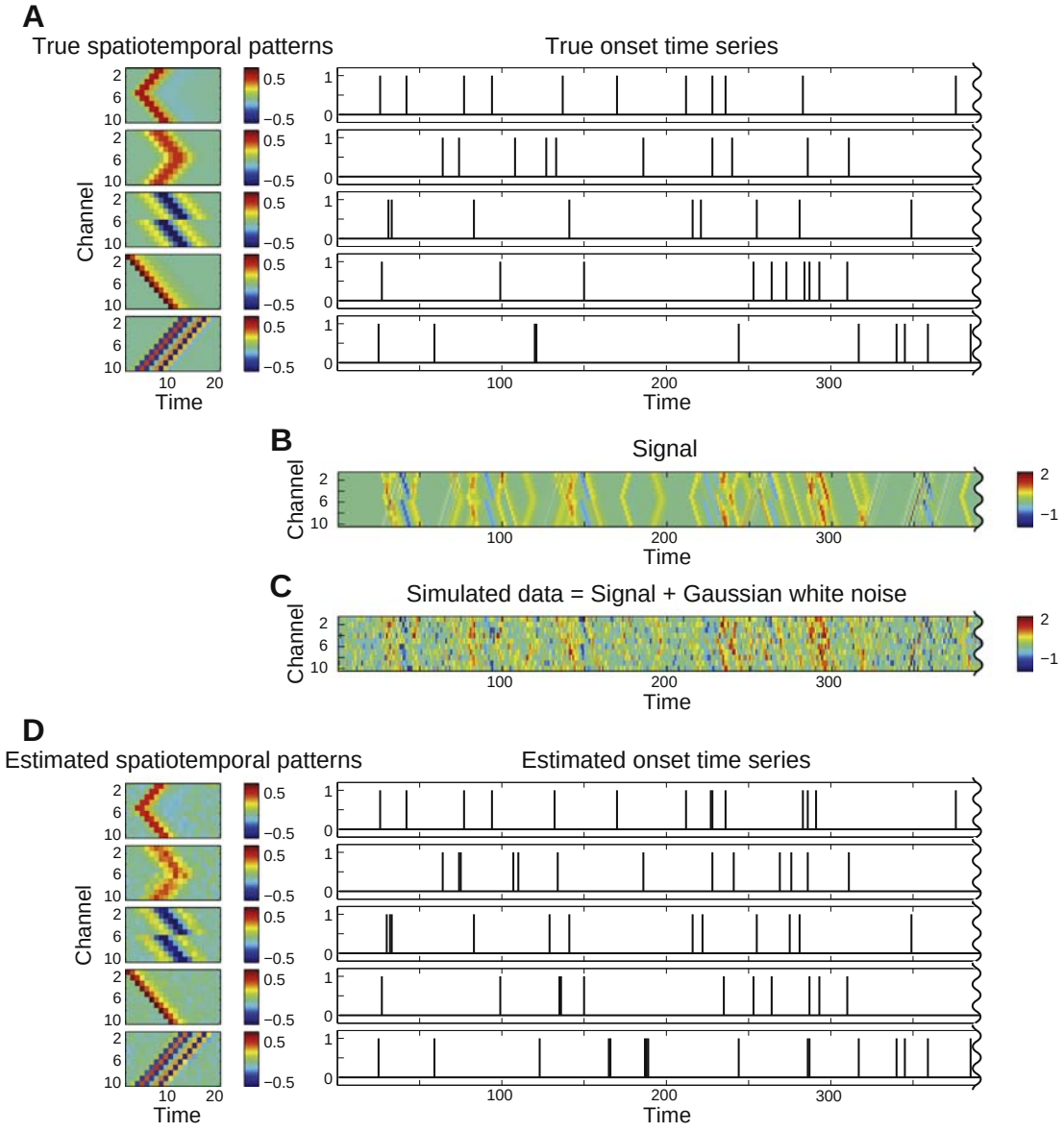

Fig. 3. Basic simulation test. (A): True spatiotemporal patterns (left) and their onset time series (right). (B): Signal time series generated by summing convolutions of true spatiotemporal patterns and their onset time series. (C): Simulated data generated by adding Gaussian white noise to signal time series. (D): Estimated spatiotemporal patterns (left) and their onset time series (right).

estimation. We changed the assignment of the estimated spatiotemporal patterns and adjusted the average of the estimated onsets so that the difference between the true and estimated spatiotemporal patterns was minimized. This procedure was also conducted when comparing spatiotemporal patterns estimated from different data or with different parameters.

Correlation coefficient of spatiotemporal patterns

To quantify the estimation accuracy of the spatiotemporal patterns, we calculated the correlation coefficients between the true and estimated spatiotemporal patterns and then averaged them across the spatiotemporal patterns.

Normalized distance from true onsets

To quantify the estimation accuracy of the onsets, we calculated two metrics: normalized distance from the true onsets and normalized number of estimated onsets. The normalized distance from the true onsets represents how close the estimated onsets are to the true ones compared to the mean inter-onset interval (IOI) of the estimated onsets, and it was calculated by

$$\frac{1}{K}\sum_{k=1}^{K}\frac{1}{a_k \times I_k}\sum_{i=1}^{I_k}\min_j |\tau_{k,i}-\hat{\tau}_{k,j}|,$$

where I_k is the number of true onsets for the k-th spatiotemporal pattern, $\tau_{k,i}$ is the i-th true onset of the k-th spatiotemporal pattern, and $\hat{\tau}_{k,j}$ is the j-th estimated onset of the k-th spatiotemporal pattern. a_k is a normalization value representing the mean IOI and is calculated by

$$a_k = \frac{1}{\hat{I}_k - 1}\sum_{i=2}^{\hat{I}_k}\left(\hat{\tau}_{k,i}-\hat{\tau}_{k,i-1}\right),$$

where $\hat{I}_k$ is the number of estimated onsets for the k-th spatiotemporal pattern. The normalized distance from the true onsets becomes close to 0 if the estimated onsets are close to the true ones.

Normalized number of estimated onsets

The normalized number of estimated onsets represents how many onsets are estimated compared to the number of true onsets, and it was calculated by

$$\frac{1}{K}\sum_{k=1}^{K}\frac{\hat{I}_k}{I_k}.$$

This value becomes larger than 1 if there are false positive onsets.

MEG

To show the applicability of STeP for real MEG data, we conducted a MEG experiment.

Eleven healthy subjects (ages 26.8 ± 7.5 years [mean ± SD]) participated in this experiment. All subjects gave written informed consent for the experimental procedures, which were approved by the ATR Human Subject Review Committee. All of them had normal or corrected-to-normal visual acuity.

The experimental design is shown in Fig. 4. A MEG recording session consisted of three 5-min consecutive periods: Rest 1, Stimulation, and Rest 2. Throughout the session, the subjects were instructed to fixate on a white cross. During Stimulation, a visual stimulus was presented 100 times with a duration of 0.1 s on the left-hand side of the white cross. The inter-stimulus intervals were 3–4 s.

The MEG were recorded with a whole-head 400-channel system (210-channel Axial Gradiometer and 190-channel Planar Gradiometer; PQ1400RM; Yokogawa Electric Co., Japan). The sampling frequency was 1 kHz. An electrooculogram (EOG) value was simultaneously recorded.

In offline analyses, the MEG data were passed through a low-pass FIR filter with a cutoff frequency of 8 Hz, sampled at 50 Hz, and passed through a high-pass FIR filter with a cutoff frequency of 1 Hz. Using reference sensor data, environmental noise was removed by time-shift Principal Component Analysis (PCA) (de Cheveigné and Simon, 2007). EOG artifacts were removed by generating a multiple linear regression model to predict eye-movement-related components in the MEG data using the EOG data, and then the prediction was removed from the MEG data. Cardiac artifacts and sensor noise were removed by ICA (Jung et al., 2001).

To examine whether STeP could estimate the VEF without using stimulus onset information, we applied STeP to the continuous MEG data during Stimulation. We used 10 axial channels where the VEF was large, and we set the length of spatiotemporal patterns to 0.5 s based on the waveform of the VEF. For each subject, we determined the number of spatiotemporal patterns based on reproducibility of estimation results. After estimating spatiotemporal patterns, we selected the spatiotemporal pattern corresponding to the VEF and adjusted the average of its estimated onsets so that the difference between the VEF and the selected spatiotemporal pattern became smallest. To quantify the similarity between the VEF and the selected spatiotemporal pattern, we calculated the correlation coefficient between them. To test the statistical significance of the correlation coefficient, we generated 1000 surrogate values for the correlation coefficient using IOI randomized onsets and calculated $p = Ns/1000$, where Ns is the number of surrogate values larger than the actual correlation coefficient. To quantify how many stimulus onsets were detected, we calculated the detection rate by $Nd/100$, where Nd is the number of trials in which the onsets were estimated between the stimulus onsets ± 0.02 s. The statistical significance of the detection rate was tested in the same way as the correlation coefficient. Furthermore, to quantify the extent to which the VEF is dominant in the MEG data, we calculated the contribution ratio of the VEF by

$$1-\frac{\sum_{ch=1}^{10}\sum_{t=1}^{T}\underline{y}^{(ch)}(t)^2}{\sum_{ch=1}^{10}\sum_{t=1}^{T}y^{(ch)}(t)^2},$$

where $\underline{y}^{(ch)}(t)$ was obtained by subtracting the VEF from the MEG data.

To estimate repetitive spatiotemporal patterns in resting-state MEG data, we applied STeP to the MEG data during Rest 1. The MEG data

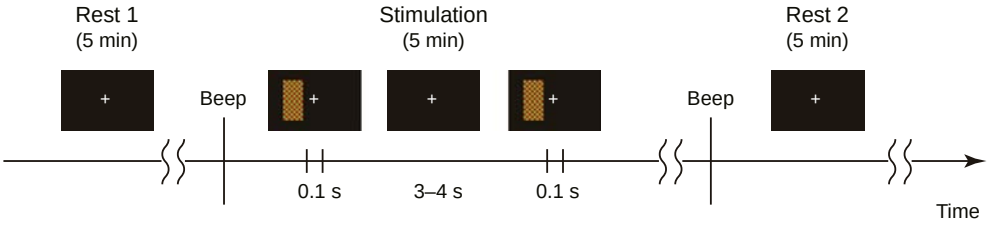

Fig. 4. Experimental design of MEG experiment. A MEG recording session consists of three consecutive periods: Rest 1, Stimulation, and Rest 2. Throughout the experiment, subjects were instructed to fixate on a white cross.

were preprocessed as described above except that the cutoff frequency of the low-pass filter was 25 Hz. We used 210 axial channels.

fMRI

To show the applicability of STeP for fMRI data, we conducted a resting-state fMRI experiment.

Ten healthy subjects (ages 29.2 ± 7.6 years) participated in this experiment. All gave written informed consent for the experimental procedures, which were approved by the ATR Human Subject Review Committee, and all had normal or corrected-to-normal visual acuity.

The experiment was done in a 10-min resting-state condition. The subjects were instructed to fixate on a white dot, to let their mind wander, and to not focus on any one thing.

Three Tesla MR scanner (MAGNETOM Trio 3 T; Siemens, Germany) was used to obtain the structural and functional MRI data. The following are the acquisition parameters for the T1-weighted images: repetition time 2300 ms, time of echo 2.98 ms, flip angle 9°, slice thickness 1 mm, field of view 256 × 256 mm, and imaging matrix 256 × 256 with 240 slices. The following are the acquisition parameters for the echo-planar images (EPIs): repetition time 2500 ms, time of echo 30 ms, flip angle 80°, slice thickness 4 mm, field of view 211.84 × 211.84 mm, and imaging matrix 64 × 64 with 40 slices.

In offline analyses, the fMRI data were preprocessed by SPM8 (Welcome Department of Cognitive Neurology, UK). Here, head motion and slice-timing were corrected. The images were spatially normalized to match the MNI template and smoothed with an 8-mm full-width at half-maximum (FWHM) Gaussian filter. The time series of each voxel was high-pass filtered to 1/128 Hz. To remove motion artifacts, we subtracted components correlated with head motion from the time series of each voxel. After normalizing the time series of each voxel to obtain a mean of 0 and an SD of 1, the preprocessed fMRI data of the gray matter for all subjects were concatenated together. To verify the effect of preprocessing, we applied both ICA and seed-based correlation analysis to the concatenated data. This revealed spatial patterns consistent with the DMN (Fox et al., 2005; Smith et al., 2009; Tong et al., 2015) (Supplementary material), suggesting the effectiveness of the preprocessing.

We then applied STeP to the concatenated fMRI data. To shorten the computation time, we used PCA to reduce the dimension of the fMRI data from the number of voxels to that of the samples while keeping its amplitude information. From this low-dimensional data, we estimated the onsets of spatiotemporal patterns. Then, using the estimated onsets, we estimated spatiotemporal patterns from the original fMRI data by Eq. (5).

Results

Basic simulation test

The performance of STeP was tested using simulated data.

We generated five spatiotemporal patterns (Fig. 3A, left) and generated their onsets using random numbers (Fig. 3A, right). By summing the convolutions of the spatiotemporal patterns and their onset time series, we obtained a signal time series (Fig. 3B). We can see that the spatiotemporal patterns are overlapping (Fig. 3B). Simulated data were generated by adding Gaussian white noise to the signal time series (Fig. 3C). The SD of the noise was set to 0.40 so that the SNR would become −5. The simulated data are too noisy to visually distinguish the spatiotemporal patterns and their onsets (Fig. 3C). We estimated the spatiotemporal patterns and their onsets by applying STeP to the simulated data (Fig. 3C). In the estimation, we set the number and length of the spatiotemporal patterns to the true values of 5 and 20, respectively. The estimation required about 8 min on a Xeon processor (3.2 GHz × 8 cores).

Fig. 3D shows the estimated spatiotemporal patterns and onsets. The estimated spatiotemporal patterns resemble the true ones (Fig. 3A and D, left) (the correlation coefficient between the true and estimated spatiotemporal patterns was 0.98). The estimated onsets are close to the true onsets (Fig. 3A and D, right), with the normalized distance from the true onsets at 0.02. The number of estimated onsets is almost the same as that of true onsets (Fig. 3A and D, right), with the normalized number of estimated onsets at 1.18. These results indicate that STeP successfully estimated the spatiotemporal patterns and their onsets from the noisy simulated data (Fig. 3C), even though the spatiotemporal patterns were overlapping.

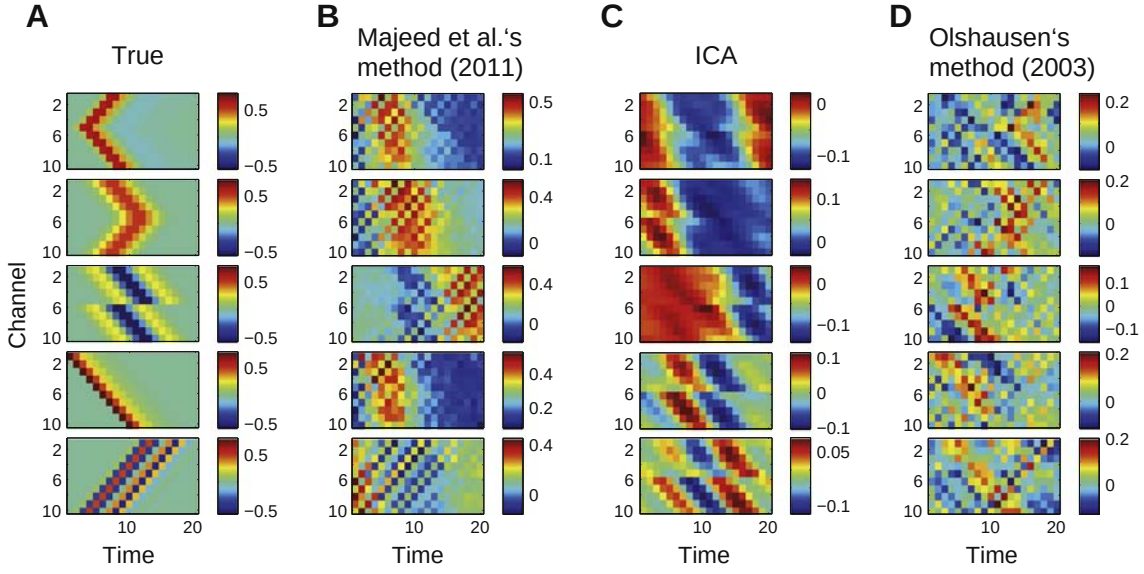

Fig. 5. Performances of three other methods. (A): True spatiotemporal patterns, which are the same as those shown in Fig. 3A, left. (B): Majeed et al.'s method (2011). Five representative templates are shown. (C): ICA. Mixing vectors of ICs were reorganized to form spatiotemporal patterns. (D): Olshausen's method (2003). Estimated basis functions are shown.

Testing other methods

To clarify the differences between STeP and other approaches, three existing methods were also applied to the same simulated data (Fig. 3C). Their performances were also quantified by the correlation coefficients between the true spatiotemporal patterns (Fig. 5A) and the estimated ones, which were ordered and shifted along time to maximize the correlation coefficients.

First, we tested Majeed et al.'s method (2011), which is basically a template-matching algorithm. Fig. 5B shows examples of the estimated templates. The estimated templates do not resemble the true spatiotemporal patterns (Fig. 5A and B) (the correlation coefficient between the true spatiotemporal patterns and the templates was 0.50). This performance is attributable to the fact that, in the simulated data, the spatiotemporal patterns are overlapping (Fig. 3B), and this method cannot separate them. In the case of STeP, overlapping spatiotemporal patterns can be separated (Fig. 3D, left).

Second, we tested ICA. To obtain spatiotemporal patterns by ICA, we first generated time-shifted data. We increased the dimension of the simulated data from CH to $CH \times N$ by treating the data at time $t-n$ ($n=1,\cdots,N-1$) as additional channels. Then, we applied ICA to the time-shifted data while regarding the time-shifted data at each time point as a sample and setting the number of ICs to 5. We used runica.m from EEGLAB, version 13.4.4b (Delorme and Makeig, 2004). The resulting mixing vectors of the ICs were reorganized to form spatiotemporal patterns ([CH,N]). Fig. 5C shows the estimated mixing vectors. The estimated mixing vectors do not resemble the true spatiotemporal patterns (Fig. 5A and C) (the correlation coefficient between the true spatiotemporal patterns and the estimated mixing vectors was 0.53). This is attributed to the fact that ICA is not designed for estimating repetitive spatiotemporal patterns.

Finally, we tested Olshausen's method (2003), which has a similar generative model and purpose as STeP. Its main difference from STeP is that $\boldsymbol{u}$ [Eq. (3)] is assumed to represent coefficients of basis functions $\boldsymbol{p}$ and takes continuous values. We applied his method to the simulated data (Fig. 3C) while setting the number of basis functions to 5. Fig. 5D shows the estimated basis functions. The estimated basis functions do not resemble the true spatiotemporal patterns (Fig. 5A and D) (the correlation coefficient between the true spatiotemporal patterns and the estimated basis functions was 0.54). This is attributable to the fact that the estimated $\boldsymbol{u}$ took continuous values as described above (not shown), although the true $\boldsymbol{u}$ took binary values (Fig. 3A, right). In the case of STeP, $\boldsymbol{u}$ is assumed to represent the onset timing of spatiotemporal patterns and should be a binary (0 or 1) value. This works as a strong constraint and improves the estimation accuracy of STeP.

Detailed simulation tests

We examined the performance of STeP in more detail. We repeatedly evaluated the estimation accuracies of spatiotemporal patterns and their onsets at the SNRs of −10, −5, and 0. The simulated data were generated with the same parameters as the first simulation test (Fig. 3) except for the SNRs. In the estimation, we set the number and length of the spatiotemporal patterns to the true values of 5 and 20, respectively. Simulation tests were conducted in 20 runs using different onsets and noise.

Fig. 6 shows the estimation accuracies quantified by the three metrics: the correlation coefficients of the spatiotemporal patterns (A), the normalized distances from the true onsets (B), and the normalized numbers of estimated onsets (C). When the SNR is 0, all three metrics show high estimation accuracies for all runs. This result indicates that, when the SNR is sufficiently high, STeP robustly estimates the spatiotemporal patterns and their onsets accurately. When the SNR is −10, the normalized numbers of estimated onsets are much larger than 1. This result indicates that, when the SNR is low, STeP estimates many false positive onsets.

In actual application, the number of spatiotemporal patterns is unknown, but we need to set it. Here, we examined the performance of STeP when the assumed number of spatiotemporal patterns was wrong. The simulated data were generated with the same parameters as the first simulation test (Fig. 3). In the estimation, we set the number of spatiotemporal patterns to either 3, 4, 5 (true), 6, or 7. The simulation tests were conducted in 2 runs using different onsets and noise. Fig. 7A shows the estimated spatiotemporal patterns in the first run. When the assumed number of spatiotemporal patterns is smaller than true (<5), some of the estimated spatiotemporal patterns seem to be contaminated with other spatiotemporal patterns. When the assumed number of spatiotemporal patterns is larger than true (>5), some of the estimated spatiotemporal patterns seem to have low SNR (Fig. 7A). To examine the reproducibility of the estimated spatiotemporal patterns, we calculated the correlation coefficients of the estimated spatiotemporal patterns between the first and second runs. Fig. 7B shows the correlation coefficients. When the assumed number of spatiotemporal patterns is larger than true (>5), some of the estimated spatiotemporal patterns show low correlation coefficients (<0.6), indicating that they had low reproducibility. This result suggests a way to determine the number of spatiotemporal patterns: examine the reproducibility of estimated spatiotemporal patterns by dividing data into two parts.

The length of spatiotemporal patterns is also unknown, but we need to set it. We examined the performance of STeP when the assumed length of spatiotemporal patterns was wrong. The simulated data were generated with the same parameters as the first simulation test (Fig. 3). In the estimation, we set the length of the spatiotemporal patterns to either 10, 15, 20 (true), 25, 30, 35, or 40. The simulation tests were conducted in 20 runs using different onsets and noise. Fig. 8A shows the correlation coefficients between the true and estimated spatiotemporal patterns. The correlation coefficients at the lengths of 15, 25, and 30 are not different from those at the length of 20 (true) ($p>0.05$, two-tailed Wilcoxon signed-rank test, Bonferroni-corrected). This result indicates that the estimation accuracy did not greatly decrease unless the assumed length of the spatiotemporal pattern was

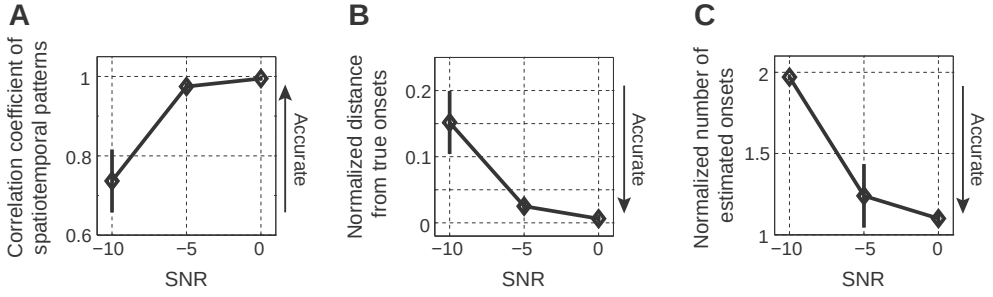

Fig. 6. Detailed performance of STeP. (A): Correlation coefficients between true and estimated spatiotemporal patterns. (B): Normalized distances from true onsets. (C): Normalized numbers of estimated onsets. In all figures, error bars represent SDs across runs.

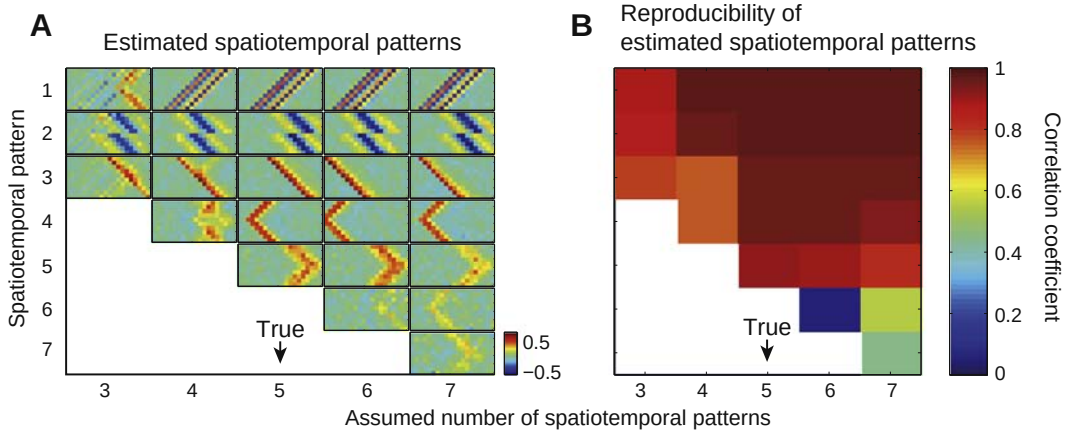

Fig. 7. Performance of STeP when assumed number of spatiotemporal patterns is wrong. (A): Estimated spatiotemporal patterns for each assumed number of spatiotemporal patterns. True number of spatiotemporal patterns is 5. (B): Reproducibility of estimated spatiotemporal patterns. Correlation coefficients of estimated spatiotemporal patterns between first and second runs are shown.

far from the true value. Therefore, we need not know the exact length of the spatiotemporal patterns.

In the case of real brain activity data, it is possible that the amplitudes of spatiotemporal patterns vary from onset to onset. To examine the performance of STeP for such data, we applied STeP to simulated data, including spatiotemporal patterns whose amplitudes are variable. The simulated data were generated with the same parameters as the first simulation test (Fig. 3), except that the spatiotemporal patterns were multiplied by $1 + w$, where w is a Gaussian white noise that is different across the onsets and spatiotemporal patterns. The SDs of w were set to 0, 0.2, 0.4, 0.6, 0.8, and 1. In the estimation, we set the number and length of the spatiotemporal patterns to the true values of 5 and 20, respectively. The simulation tests were conducted in 20 runs for each SD of w using different onsets and noise. Fig. 8B shows the correlation coefficients between the true and estimated spatiotemporal patterns as a function of the SDs of w. The correlation coefficients at SD $= 0.2$, 0.4, 0.6, 0.8, and 1 are not different from those at SD $= 0$ ($p > 0.05$, two-tailed Wilcoxon signed-rank test, Bonferroni-corrected). This result indicates that the variability of the amplitudes did not greatly decrease the estimation accuracy. This is because, as the variability of the amplitudes becomes large, huge spatiotemporal patterns sometimes appear and STeP easily detects them while missing small ones. For the VEF shown in Fig. 9C, the SD of w was estimated at 0.36. Considering these results, the variability of the amplitudes of spatiotemporal patterns is considered no problem for STeP.

Performance test with real MEG data

We examined the performance of STeP with real MEG data. It is generally believed that repeated presentation of a visual stimulus evokes a stereotypical MEG pattern, the so-called VEF. STeP is proposed to estimate such stereotypical spatiotemporal patterns without using their onset information. Therefore, we tested whether STeP could estimate the VEF without using the stimulus onset information.

We applied STeP to the continuous MEG data during Stimulation (Fig. 4) at 10 axial channels where the VEFs are large. We set the length of spatiotemporal patterns to 0.5 s based on the waveforms of the VEFs. For each subject, we determined the number of spatiotemporal patterns based on the reproducibility of the estimation results. Fig. 9 shows the results of one subject. Fig. 9A shows the 10 selected channels. To determine the number of spatiotemporal patterns, we divided the MEG data into two parts, each of which was 2.5-min data, and estimated spatiotemporal patterns separately while setting the number of spatiotemporal patterns to either 1, 2, 3, 4, or 5. Fig. 9B shows the correlation coefficients between the spatiotemporal patterns separately estimated from the two parts. When the assumed number of spatiotemporal patterns is larger than 1, some of the estimated spatiotemporal patterns

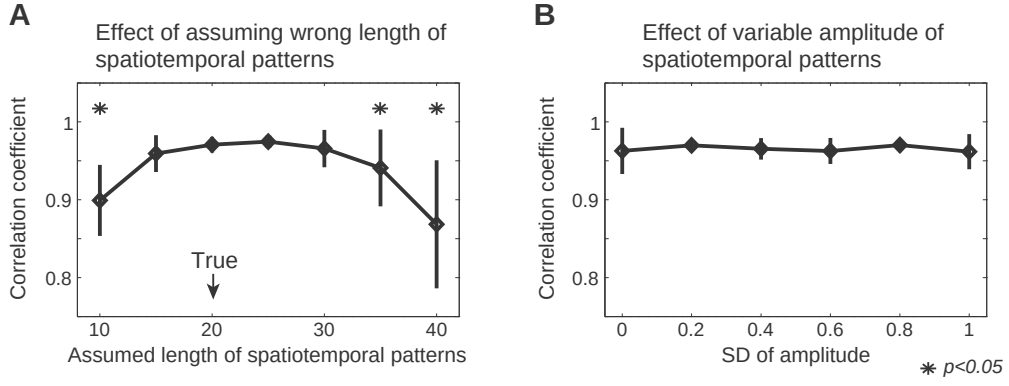

Fig. 8. Performance of STeP when our assumption is not correct. (A): Performance of STeP when assumed length of spatiotemporal patterns is wrong. True length of spatiotemporal patterns is 20. Correlation coefficients between true and estimated spatiotemporal patterns are shown. (B): Performance of STeP when amplitudes of spatiotemporal patterns are variable. Correlation coefficients between true and estimated spatiotemporal patterns are shown. Horizontal axis represents SD of w, where spatiotemporal patterns were multiplied by $1 + w$. In both figures, error bars represent SDs of correlation coefficients across runs.

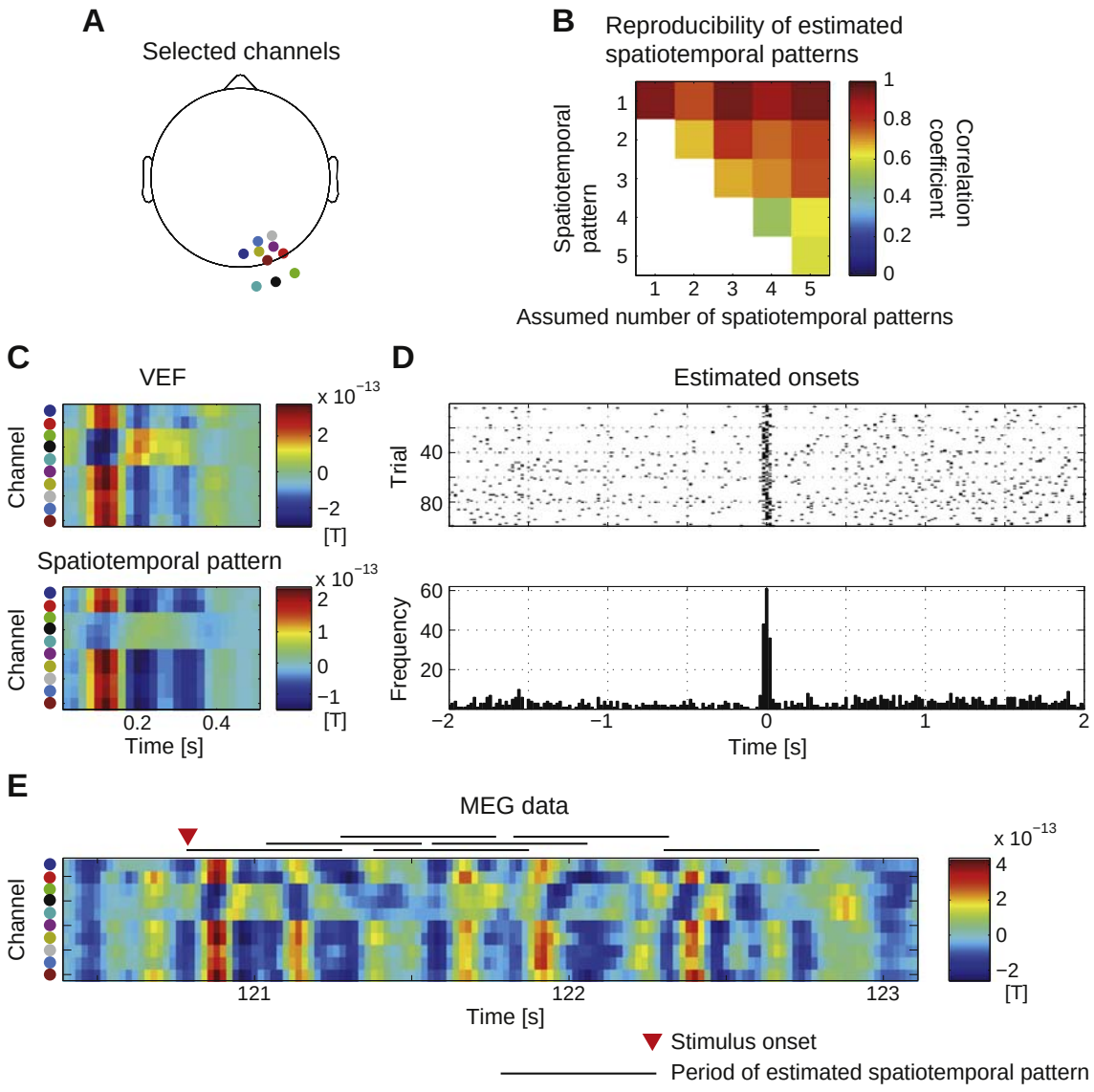

Fig. 9. Estimation accuracy of a subject's VEF. (A): Selected 10 channels. (B): Reproducibility of estimated spatiotemporal patterns. Correlation coefficients between spatiotemporal patterns separately estimated from the two parts of the divided data are shown. Based on this result, we set the number of spatiotemporal patterns to 1 for this subject. (C): VEF (top) and estimated spatiotemporal pattern (bottom). (D): Raster plot (top) and histogram (bottom) of estimated onsets. Time 0 corresponds to stimulus onsets. (E): Example of MEG data at 10 selected channels. Red triangle indicates a stimulus onset. Black bars indicate periods of estimated spatiotemporal pattern, onsets of which correspond to estimated onsets. In (C) and (E), locations of channels are indicated by color in (A).

show low correlation coefficients (<0.7), that is, these patterns have low reproducibility. Therefore, we set the number of spatiotemporal patterns to 1 for this subject. Fig. 9C shows the VEF (top), which was obtained by averaging the MEG data triggered at the stimulus onsets, and the estimated spatiotemporal pattern (bottom) obtained by setting the number of spatiotemporal patterns to 1. The estimated spatiotemporal pattern resembles the VEF (the correlation coefficient between them is 0.90, $p<0.01$). Fig. 9D shows the raster plot (top) and histogram (bottom) of the estimated onsets, which were generated by segmenting the estimated onset time series triggered at the stimulus onsets. A large number of onsets were estimated around time 0, corresponding to the stimulus onsets. The detection rate of the stimulus onsets is 0.92 ($p<0.01$), indicating that STeP detected the stimulus onsets at a significantly high rate. These results indicate that STeP successfully estimated the VEF without using the stimulus onset information.

Actually, many onsets were estimated far from the stimulus onsets (Fig. 9D). In fact, at the estimated onsets far from the stimulus onsets, there seems to be a spatiotemporal pattern resembling the estimated one (Fig. 9E, see MEG data under black bars). Han et al. (2008) showed that visually evoked cortical activity reverberates in subsequent spontaneous waves. The estimated onsets far from the stimulus may reflect the reverberation.

The estimation results of all subjects are summarized in Fig. 10. These figures show scatter plots of the contribution ratios of the VEFs and the two metrics, i.e. the correlation coefficients between the VEFs and the estimated spatiotemporal pattern (A), as well as the detection rates of the stimulus onsets (B). Each dot corresponds to each subject, and its color represents the number of spatiotemporal patterns determined based on the reproducibility of the estimation results. The correlation coefficients and the detection rates are higher than 0.8 for the subjects whose contribution ratios of the VEFs are larger than 0.1. This indicates that STeP successfully estimated the VEFs and their onsets, unless the VEFs were too small. It is assumed that, when the VEFs were too small, STeP estimated more dominant spatiotemporal patterns than the VEFs.

In summary, STeP can estimate the VEF without using any stimulus onset information, indicating the applicability of STeP for real MEG data.

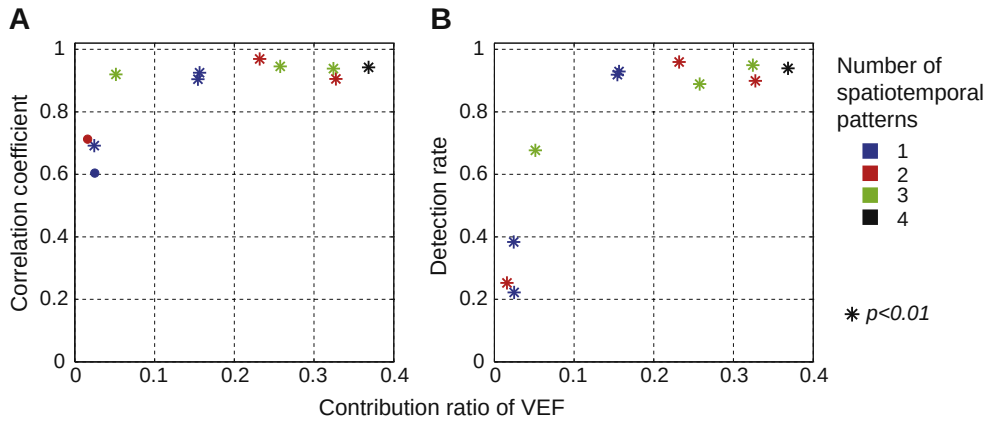

Fig. 10. Estimation accuracies of all subjects' VEFs. (A): Scatter plots of contribution ratios of VEFs and correlation coefficients between VEFs and estimated spatiotemporal patterns. (B): Scatter plots of contribution ratios of VEFs and detection rates of stimulus onsets. In both figures, each dot corresponds to one subject, and its color represents the number of spatiotemporal patterns determined based on the reproducibility of estimation results. Significantly large values are indicated by asterisks.

Application to resting-state fMRI data

To demonstrate the usefulness of STeP, we applied it to the resting-state fMRI data.

To determine the number of spatiotemporal patterns, we first examine the reproducibility of estimated spatiotemporal patterns. We divided the resting-state fMRI data into two parts, each of which contained five subjects' data, and estimated spatiotemporal patterns separately while setting the number of spatiotemporal patterns to either 1, 2, 3, 4, or 5. The length of spatiotemporal patterns was set to 10 s. Fig. 11A shows the correlation coefficients between the spatiotemporal patterns separately estimated from the two parts. When the assumed number of spatiotemporal patterns is larger than 2, some of the estimated spatiotemporal patterns show low correlation coefficients (<0.7), that is, these patterns have low reproducibility. Therefore, we decided to set the number of the spatiotemporal patterns to 2. Furthermore, we assessed the sensitivity of the estimation results to the assumed length of the spatiotemporal patterns. From the whole resting-state fMRI data, which contains ten subjects' data, we estimated the spatiotemporal patterns while setting the length of the spatiotemporal patterns to either 5, 7.5, 10, 12.5, or 15 s. The number of spatiotemporal patterns was set to 2. Fig. 11B shows the pairwise correlation coefficients between the estimated spatiotemporal patterns of different lengths. When the length of the spatiotemporal pattern is longer than 5 s, the correlation coefficients are constantly high (>0.8). This indicates that the estimation results were not sensitive to the assumed length of the spatiotemporal pattern if it was larger than 5 s.

Fig. 12A shows the spatiotemporal patterns obtained by setting the number and length of the spatiotemporal patterns to 2 and 10 s, respectively. The two spatiotemporal patterns show positive and negative activities, respectively. In both patterns, the spatial patterns at 10 s seem to reflect large activities at veins, suggesting that these spatial patterns reflect the cerebral venous drainage. Furthermore, in both patterns, regions belonging to the same resting-state networks (RSNs) show large activities at the same time points: 5 s for auditory, 7.5 s for visual and cerebellum (Smith et al., 2009). This is reasonable because an RSN consists of co-activating regions. Tong et al. (2012, 2015) showed that systemic low-frequency oscillations (sLFOs) travel through the entire brain and reach different voxels with different delays. The propagation pattern in the estimated spatiotemporal patterns (Fig. 12A), from the auditory cortex to veins via the visual and cerebellum cortices, seems to be consistent with the delay map of sLFOs (Fig. 3A in Tong et al., 2015).

For comparison, we also applied Majeed et al.'s method (2011) to the same resting-state fMRI data. The length of the template was set to 10 s. Fig. 12B shows the template estimated by Majeed et al.'s method (2011). The spatial pattern at 10 s in the template resembles the spatial pattern at 5 s in the first spatiotemporal pattern (the correlation coefficient between them was 0.87) (Fig. 12A, left and B). The spatial pattern at 2.5 s in the template resembles the spatial pattern at 7.5 s in the second spatiotemporal pattern (the correlation coefficient

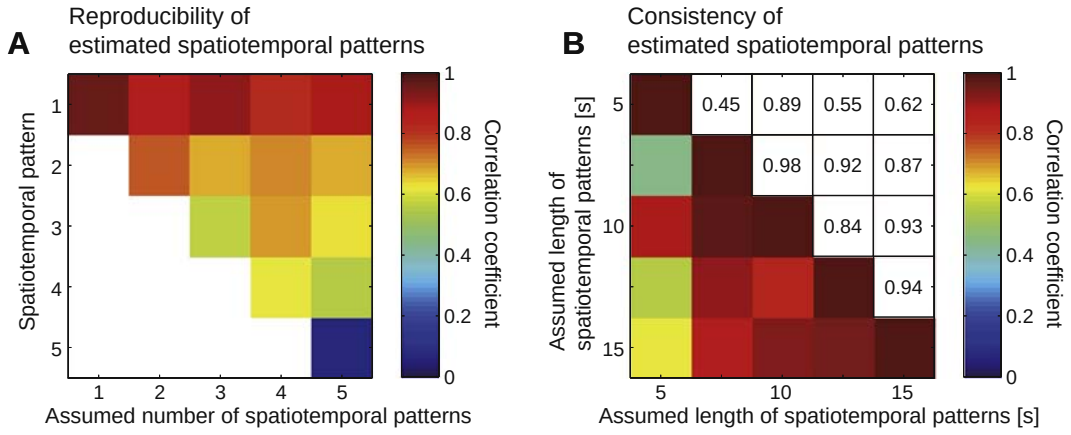

Fig. 11. Effects of assumed number and length of spatiotemporal patterns on estimation results from resting-state fMRI. (A): Effects of assumed number of spatiotemporal patterns on reproducibility of estimation results. Correlation coefficients between spatiotemporal patterns separately estimated from the two parts of the divided data are shown. (B): Effects of assumed length of spatiotemporal patterns on estimation results. Pairwise correlation coefficients between estimated spatiotemporal patterns of different lengths are shown.

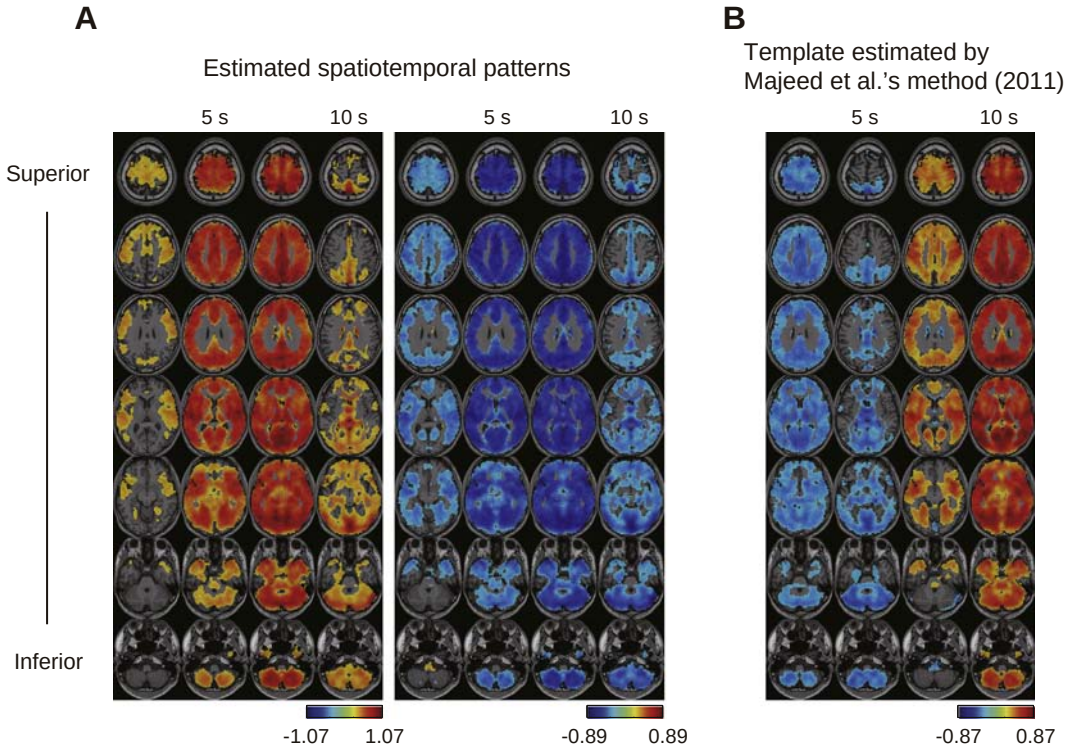

Fig. 12. Spatiotemporal patterns estimated from resting-state fMRI data concatenated across all subjects. (A): Two spatiotemporal patterns estimated by STeP. (B): Template estimated by Majeed et al.'s method (2011). In these figures, activities whose absolute values are over 0.3 of maximum value across voxels are shown.

between them was 0.83) (Fig. 12A, right and B). These similarities suggest the validity of the estimated spatiotemporal patterns.

Application to resting-state MEG data

We also applied STeP to the resting-state MEG data. Here, we show the estimation results of a subject.

To determine the number of spatiotemporal patterns, we first examine the reproducibility of estimated spatiotemporal patterns. We divided the resting-state MEG data into two parts, each of which was 2.5-min data, and estimated spatiotemporal patterns separately while setting the number of spatiotemporal patterns to either 1, 2, 3, 4, or 5. The length of spatiotemporal patterns was set to 0.5 s. Fig. 13A shows the correlation coefficients between the spatiotemporal patterns separately estimated from the two parts. When the assumed number of spatiotemporal patterns is larger than 1, all of the estimated spatiotemporal patterns show low correlation coefficients (<0.7). Therefore, we decided to set the number of spatiotemporal patterns to 1. Furthermore, we assessed the sensitivity of the estimation results to the assumed length of the spatiotemporal pattern. From the whole resting-state MEG data, we estimated the spatiotemporal patterns while setting the length of the spatiotemporal patterns to either 0.2, 0.3, 0.4, 0.5, 0.6, 0.7, or 0.8 s. The number of spatiotemporal patterns was set to 1. Fig. 13B shows the pairwise correlation coefficients between the estimated spatiotemporal patterns of the different lengths. When the length of the spatiotemporal pattern is longer than 0.2 s, the correlation coefficients are constantly high (>0.7). This indicates that the estimation results were not so sensitive to the assumed length of the spatiotemporal pattern if it was larger than 0.2 s.

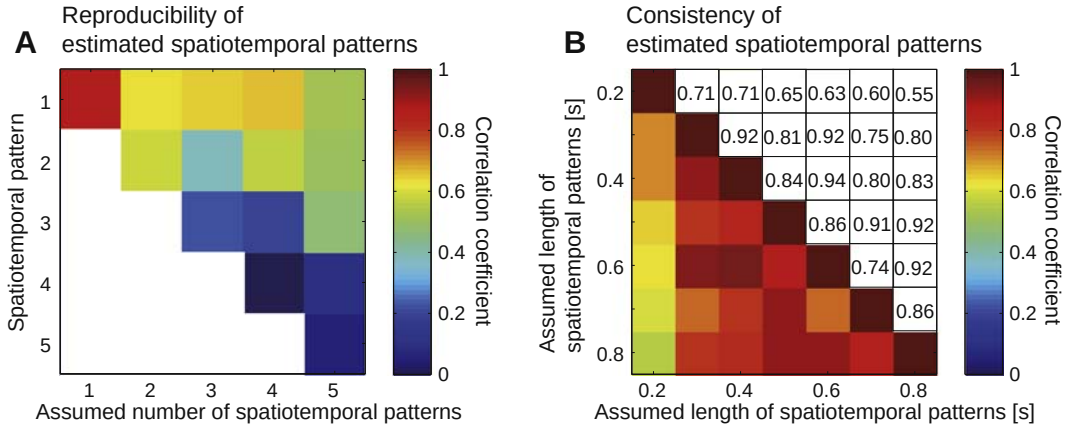

Fig. 13. Effects of assumed number and length of spatiotemporal patterns on estimation results from resting-state MEG. (A): Effects of assumed number of spatiotemporal patterns on reproducibility of estimation results. Correlation coefficients between spatiotemporal patterns separately estimated from the two parts of the divided data are shown. (B): Effects of assumed length of spatiotemporal patterns on estimation results. Pairwise correlation coefficients between spatiotemporal patterns of different lengths are shown.

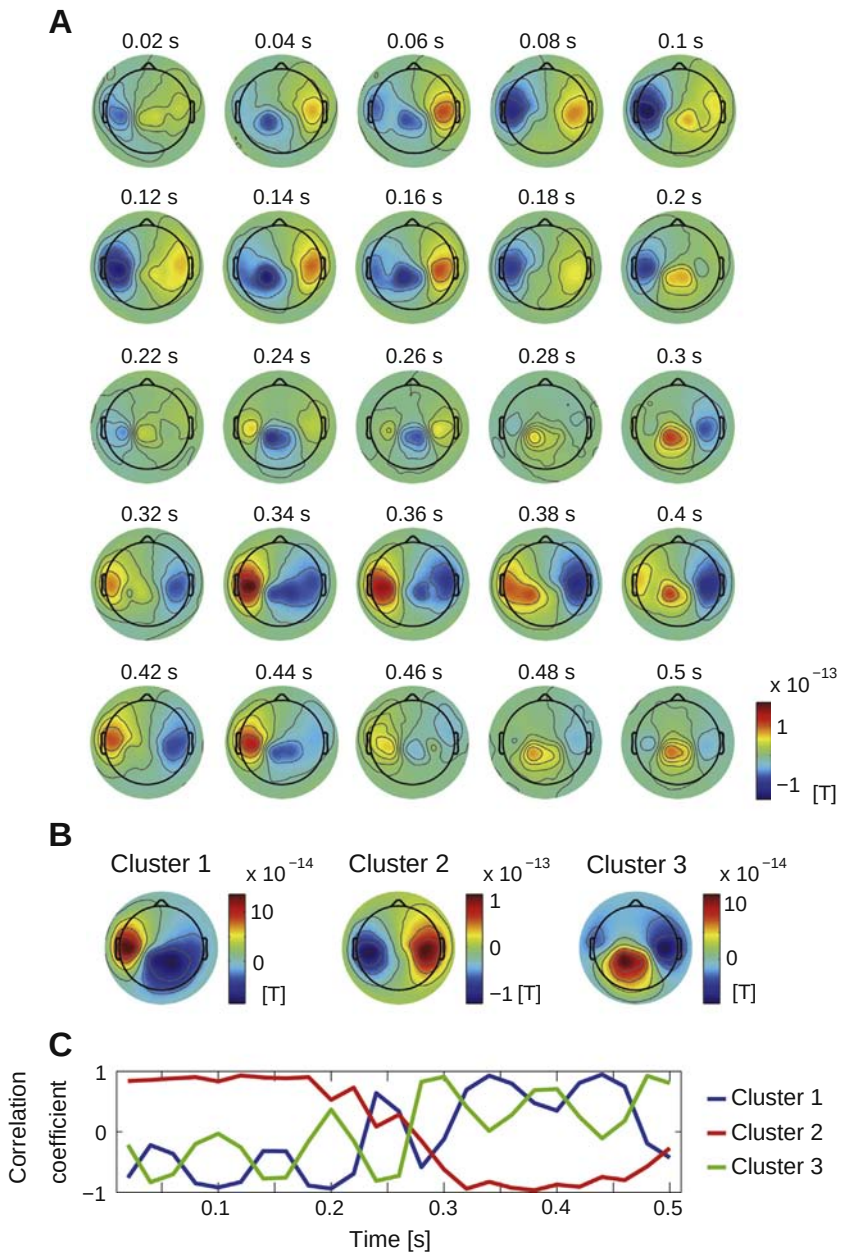

Fig. 14. Spatiotemporal pattern estimated from a subject's resting-state MEG data. (A): Spatiotemporal pattern. (B): Centers of clusters estimated by k-means clustering. (C): Correlation coefficients between spatiotemporal pattern at each time (A) and centers of clusters (B).

Fig. 14A shows the spatiotemporal pattern obtained by setting the number and length of the spatiotemporal patterns to 1 and 0.5 s, respectively. The spatiotemporal pattern contains spatial patterns similar to the movement-related magnetic fields at 0.20, 0.24, 0.34 and 0.44 s.

For comparison, we also applied k-means clustering (MacQueen, 1967) to the same resting-state MEG data. Here, the resting-state MEG data at each time point was regarded as a sample, and the number of clusters was set to 3. Fig. 14B shows the centers of the estimated clusters (Clusters 1–3). Fig. 14C shows the correlation coefficients between the spatiotemporal pattern at each time and the centers of the clusters. All of the clusters have correlation coefficients close to 1 at different time points (0.44 s for Cluster 1, 0.12 s for Cluster 2, and 0.48 s for Cluster 3), indicating the consistency between the results of STeP and k-means clustering. On the other hand, the correlation coefficients are not constant but change with time. This indicates that the spatiotemporal pattern represents the consecutive brain activities that dynamically change with time, while each cluster represents a snapshot of them.

Discussion

In this study, we proposed the STeP method to estimate repetitive spatiotemporal patterns from resting-state brain activity data. The performance tests with the simulated data show that STeP can estimate spatiotemporal patterns accurately without using their onsets, even if they are overlapping (Fig. 3). Furthermore, our results also show that STeP works robustly in various situations (Figs. 6 and 8). The performance tests with real MEG data show that STeP can estimate the VEFs without using stimulus onset information (Figs. 9 and 10). Finally, STeP was applied to the resting-state fMRI and MEG data. This revealed informative spatiotemporal patterns, showing how the brain activities dynamically change with time (Figs. 12 and 14). These results indicate the applicability and usefulness of STeP for resting-state brain activity data.

Methodological considerations

STeP searches for spatiotemporal patterns and their onsets that minimize the objective function [Eq. (4)]. This is a difficult optimization problem because there are many local minima. To solve this optimization problem, we developed the algorithm shown in Fig. 2. In this algorithm, each onset is updated sequentially (Fig. 2A, bottom level), so it is time-consuming. However, it is also possible to update all of the onsets together. For example, deconvolving spatiotemporal patterns out of resting-state data provides the information of all onsets at once. Actually, in our simulation tests (not shown) this deconvolving algorithm was very fast. However, its estimation accuracy was low because it was always trapped in local minima. Other algorithms that update all of the onsets together have shown similar results. Considering both the computational cost and the optimization performance, the proposed algorithm (Fig. 2) is empirically the best among all those we tested.

The performance tests with the simulated data show that, when SNR is low, estimated onsets include many false positives (Fig. 6C); in other words, overfitting occurs. A solution to this problem could be adding a regularization term to the objective function [Eq. (4)]. Imposing a penalty for increasing the number of onsets by a regularization term may suppress the false positive onsets and increase the estimation accuracy. Overfitting also occurs when the assumed number of spatiotemporal patterns is larger than the actual value (Fig. 7A). In this study, we suggest a solution to this problem: determine the number of spatiotemporal patterns based on the reproducibility of estimated spatiotemporal patterns (Fig. 7B). On the other hand, if our model [Eq. (3)] is reformulated with a probabilistic model, we could avoid overfitting using well-known criteria, such as Akaike's information criterion (AIC) (Akaike, 1974), the Bayesian information criterion (BIC) (Schwarz, 1978), and the free energy.

Reliability of estimation results

STeP estimates repetitive spatiotemporal patterns and their onsets if they exist. However, even if they do not exist, STeP is forced to extract spatiotemporal patterns so that the residual error [Eq. (4)] becomes small. Therefore, it is necessary to test the reliability of estimated spatiotemporal patterns and onsets.

The reliability of estimated spatiotemporal patterns could be tested by examining their reproducibility. As shown in this study (Figs. 7B, 9B, 11A, and 13A), reproducibility can be examined by estimating the spatiotemporal patterns from two separate sets of data and assessing the similarity between them. If reproducibility is high, the estimated spatiotemporal patterns could be considered reliable. Furthermore, the reproducibility of estimated spatiotemporal patterns could be a criterion for determining the number of spatiotemporal patterns (Figs. 7B, 9B, 11A, and 13A).

The reliability of estimated onsets could be tested by examining the data at estimated onsets (see Fig. 9E). If the data at an estimated onset is similar to the corresponding spatiotemporal pattern, the estimated onset could be considered reliable. This similarity can be quantified by the correlation coefficients.

Relation to other methods

For spike and fMRI data, template-matching algorithms have been applied to estimate repetitive spatiotemporal patterns (Ikegaya et al., 2004; Majeed et al., 2011). The template-matching algorithms use a segment starting at a random time point as a template. Therefore, the segment must contain a pure spatiotemporal pattern that is not overlapping with others. Otherwise, the template-matching algorithms estimate spatiotemporal patterns contaminated by each other (Fig. 5B). Because spatiotemporal patterns are assumed to overlap in the case of MEG/EEG data, the template-matching algorithms are not suitable for these data.

ICA (Beckmann et al., 2005) and clustering methods, such as k-means clustering (MacQueen, 1967), are very powerful tools to analyze resting-state brain activity data. However, these methods do not provide spatiotemporal patterns, which are two-dimensional matrices of channel × time (see Fig. 1A). Therefore, these methods do not meet our needs.

If ICA or k-means clustering is applied to time-shifted data, which are obtained by treating the data at time $t-n$ $(n=1,\cdots,N-1)$ as additional channels, the resulting mixing matrices of ICs or the centers of clusters can be regarded as spatiotemporal patterns. However, mixing matrices of ICs or centers of clusters do not necessarily reflect actual spatiotemporal patterns (Fig. 5C). This is because neither ICA nor k-means is designed to estimate repetitive spatiotemporal patterns. Therefore, applying ICA or k-means clustering to time-shifted data is not suitable for our purpose.

The methods of Olshausen (2003) and Anemüller et al. (2003) have similar generative models and purposes as ours. STeP is different from these methods mainly in the assumption of $\boldsymbol{u}$ [Eq. (3)]. In these methods, $\boldsymbol{u}$ takes continuous values, assuming that $\boldsymbol{u}$ represents coefficients of bases. In STeP, on the contrary, $\boldsymbol{u}$ takes a binary (0 or 1) value, assuming that $\boldsymbol{u}$ represents the onset timings of discrete events in the brain. To extract discrete events in the brain, our assumption is considered better (Fig. 5D).

Recently, we proposed a general method to estimate MEG/EEG waveforms that are common across trials (Common Waveform Estimation, CWE) (Takeda et al., 2010, 2014). CWE can also estimate spatiotemporal patterns even if their onsets are unknown. STeP is different from CWE mainly in the assumed data structure. CWE is used for trial data (channel × time × trial), while STeP is used for continuous data (channel × time). Because resting-state data are continuous, CWE cannot be used.

Using clustering methods and hidden Markov models, resting-state MEG/EEG data have been segmented into stationary states (e.g. microstates) (Baker et al., 2014; Britz et al., 2010; Van de Ville et al., 2010; Woolrich et al., 2013). The differences between STeP and these approaches are particularly evident when propagations occur. If brain activities propagate across different regions (e.g. from V1 to MT), the MEG/EEG spatial pattern consecutively changes with time. In this case, STeP represents it with a spatiotemporal pattern, while these approaches represent it by a transition across states. Therefore, STeP is considered suitable for capturing propagations of brain activities.

Spatiotemporal patterns in resting-state fMRI data

Using STeP, we estimated the two spatiotemporal patterns from the resting-state fMRI data (Fig. 12A). The spatiotemporal patterns show that the large activities propagate from the auditory cortex to veins via the visual and cerebellum cortices (Fig. 12A). Recently, Tong et al. (2012, 2015) showed that fMRI data are strongly contaminated with sLFOs, which are observed at peripheral sites (e.g. fingertip). They also showed that sLFOs reach different brain regions with different delays (Tong et al., 2012, 2015) and the delays are partially responsible for the emergence of RSNs (Tong et al., 2015). It is believed that the delays reflect the cerebral blood flow formed by vascular anatomy. The propagation pattern in the estimated spatiotemporal patterns (Fig. 12A) seems to be consistent with the delay map of sLFOs (Fig. 3A in Tong et al., 2015). Therefore, we suggest that the spatiotemporal patterns represent how fMRI activities propagate along the cerebral blood flow, while their origins, whether neuronal or non-neuronal, are not clear.

Applicability

Thinking of an issue, remembering the past, and imagining the future: These activities occur spontaneously and are important brain functions for human beings. However, their details are still veiled because they occur silently in our brain without exhibiting overt signs. STeP

can detect such events from various types of resting-state data, so it could help us to unveil their mechanisms.

Moreover, applying STeP to continuous data during "tasks" may also bring interesting results. Usually, continuous MEG/EEG data during tasks are segmented into trials, and the data during inter-trial intervals are discarded. However, it is possible that important brain activities also occur during inter-trial intervals. If so, applying STeP could bring us important findings. Indeed, we applied STeP to the continuous MEG data during the visual stimulation task and found that a spatiotemporal pattern resembling the VEF appears not only after the stimulus onsets but also during the inter-trial intervals (Fig. 9E).

A MATLAB implementation of the proposed method is available from http://www.cns.atr.jp/takeda/STeP.html.

Acknowledgments

The authors thank Dr. Aapo Hyvärinen for his helpful comments. This research was supported by contracts with the National Institute of Information and Communications Technology entitled, "Multimodal integration for brain imaging measurements" (13601) and "Development of network dynamics modeling methods for human brain data simulation systems" (173), and JSPS KAKENHI Grant Number 23700499.

Appendix A. Supplementary data

Supplementary data to this article can be found online at http://dx.doi.org/10.1016/j.neuroimage.2016.03.014.

References

Akaike, H., 1974. A new look at the statistical model identification. IEEE Trans. Autom. Control AC-19, 716–723.
Anemüller, J., Sejnowski, T.J., Makeig, S., 2003. Complex independent component analysis of frequency-domain electroencephalographic data. Neural Netw. 16, 1311–1323.
Baker, A.P., Brookes, M.J., Rezek, I.A., Smith, S.M., Behrens, T., Probert Smith, P.J., Woolrich, M., 2014. Fast transient networks in spontaneous human brain activity. Elife 3, e01867.
Beckmann, C.F., DeLuca, M., Devlin, J.T., Smith, S.M., 2005. Investigations into resting-state connectivity using independent component analysis. Philos. Trans. R. Soc. Lond. Ser. B Biol. Sci. 360, 1001–1013.
Biswal, B., Yetkin, F.Z., Haughton, V.M., Hyde, J.S., 1995. Functional connectivity in the motor cortex of resting human brain using echo-planar MRI. Magn. Reson. Med. 34, 537–541.
Biswal, B.B., Mennes, M., Zuo, X.N., Gohel, S., Kelly, C., Smith, S.M., Beckmann, C.F., Adelstein, J.S., Buckner, R.L., Colcombe, S., Dogonowski, A.M., Ernst, M., Fair, D., Hampson, M., Hoptman, M.J., Hyde, J.S., Kiviniemi, V.J., Kotter, R., Li, S.J., Lin, C.P., Lowe, M.J., Mackay, C., Madden, D.J., Madsen, K.H., Margulies, D.S., Mayberg, H.S., McMahon, K., Monk, C.S., Mostofsky, S.H., Nagel, B.J., Pekar, J.J., Peltier, S.J., Petersen, S.E., Riedl, V., Rombouts, S.A., Rypma, B., Schlaggar, B.L., Schmidt, S., Seidler, R.D., Siegle, G.J., Sorg, C., Teng, G.J., Veijola, J., Villringer, A., Walter, M., Wang, L., Weng, X.C., Whitfield-Gabrieli, S., Williamson, P., Windischberger, C., Zang, Y.F., Zhang, H.Y., Castellanos, F.X., Milham, M.P., 2010. Toward discovery science of human brain function. Proc. Natl. Acad. Sci. U. S. A. 107, 4734–4739.
Britz, J., Van De Ville, D., Michel, C.M., 2010. BOLD correlates of EEG topography reveal rapid resting-state network dynamics. NeuroImage 52, 1162–1170.
Brookes, M.J., Woolrich, M., Luckhoo, H., Price, D., Hale, J.R., Stephenson, M.C., Barnes, G.R., Smith, S.M., Morris, P.G., 2011. Investigating the electrophysiological basis of resting state networks using magnetoencephalography. Proc. Natl. Acad. Sci. U. S. A. 108, 16783–16788.
de Cheveigné, A., Simon, J.Z., 2007. Denoising based on time-shift PCA. J. Neurosci. Methods 165, 297–305.
de Pasquale, F., Della Penna, S., Snyder, A.Z., Lewis, C., Mantini, D., Marzetti, L., Belardinelli, P., Ciancetta, L., Pizzella, V., Romani, G.L., Corbetta, M., 2010. Temporal dynamics of spontaneous MEG activity in brain networks. Proc. Natl. Acad. Sci. U. S. A. 107, 6040–6045.
de Pasquale, F., Della Penna, S., Snyder, A.Z., Marzetti, L., Pizzella, V., Romani, G.L., Corbetta, M., 2012. A cortical core for dynamic integration of functional networks in the resting human brain. Neuron 74, 753–764.
Delorme, A., Makeig, S., 2004. EEGLAB: an open source toolbox for analysis of single-trial EEG dynamics including independent component analysis. J. Neurosci. Methods 134, 9–21.
Deuker, L., Olligs, J., Fell, J., Kranz, T.A., Mormann, F., Montag, C., Reuter, M., Elger, C.E., Axmacher, N., 2013. Memory consolidation by replay of stimulus-specific neural activity. J. Neurosci. 33, 19373–19383.
Dragoi, G., Tonegawa, S., 2011. Preplay of future place cell sequences by hippocampal cellular assemblies. Nature 469, 397–401.
Dragoi, G., Tonegawa, S., 2013. Distinct preplay of multiple novel spatial experiences in the rat. Proc. Natl. Acad. Sci. U. S. A. 110, 9100–9105.
Foster, D.J., Wilson, M.A., 2006. Reverse replay of behavioural sequences in hippocampal place cells during the awake state. Nature 440, 680–683.
Fox, M.D., Raichle, M.E., 2007. Spontaneous fluctuations in brain activity observed with functional magnetic resonance imaging. Nat. Rev. Neurosci. 8, 700–711.
Fox, M.D., Snyder, A.Z., Vincent, J.L., Corbetta, M., Van Essen, D.C., Raichle, M.E., 2005. The human brain is intrinsically organized into dynamic, anticorrelated functional networks. Proc. Natl. Acad. Sci. U. S. A. 102, 9673–9678.
Han, F., Caporale, N., Dan, Y., 2008. Reverberation of recent visual experience in spontaneous cortical waves. Neuron 60, 321–327.
Hopfield, J.J., 1995. Pattern recognition computation using action potential timing for stimulus representation. Nature 376, 33–36.
Ikegaya, Y., Aaron, G., Cossart, R., Aronov, D., Lampl, I., Ferster, D., Yuste, R., 2004. Synfire chains and cortical songs: temporal modules of cortical activity. Science 304, 559–564.
Izhikevich, E.M., 2006. Polychronization: computation with spikes. Neural Comput. 18, 245–282.
Ji, D., Wilson, M.A., 2007. Coordinated memory replay in the visual cortex and hippocampus during sleep. Nat. Neurosci. 10, 100–107.
Jung, T.P., Makeig, S., Westerfield, M., Townsend, J., Courchesne, E., Sejnowski, T.J., 2001. Analysis and visualization of single-trial event-related potentials. Hum. Brain Mapp. 14, 166–185.
MacQueen, J., 1967. Some methods for classification and analysis of multivariate observations. In: LeCam, L.M., Neyman, J. (Eds.), Proceedings of the Fifth Berkeley Symposium on Mathematical Statistics and Probability 1. University of California Press, pp. 281–297.
Majeed, W., Magnuson, M., Hasenkamp, W., Schwarb, H., Schumacher, E.H., Barsalou, L., Keilholz, S.D., 2011. Spatiotemporal dynamics of low frequency BOLD fluctuations in rats and humans. NeuroImage 54, 1140–1150.
Mantini, D., Perrucci, M.G., Del Gratta, C., Romani, G.L., Corbetta, M., 2007. Electrophysiological signatures of resting state networks in the human brain. Proc. Natl. Acad. Sci. U. S. A. 104, 13170–13175.
Olshausen, B.A., 2003. Learning sparse, overcomplete representations of time-varying natural images. IEEE International Conference on Image Processing.
Raichle, M.E., MacLeod, A.M., Snyder, A.Z., Powers, W.J., Gusnard, D.A., Shulman, G.L., 2001. A default mode of brain function. Proc. Natl. Acad. Sci. U. S. A. 98, 676–682.
Schwarz, G., 1978. Estimating the dimension of a model. Ann. Stat. 6, 461–464.
Smith, S.M., Fox, P.T., Miller, K.L., Glahn, D.C., Fox, P.M., Mackay, C.E., Filippini, N., Watkins, K.E., Toro, R., Laird, A.R., Beckmann, C.F., 2009. Correspondence of the brain's functional architecture during activation and rest. Proc. Natl. Acad. Sci. U. S. A. 106, 13040–13045.
Staresina, B.P., Alink, A., Kriegeskorte, N., Henson, R.N., 2013. Awake reactivation predicts memory in humans. Proc. Natl. Acad. Sci. U. S. A. 110, 21159–21164.
Takeda, Y., Sato, M., Yamanaka, K., Nozaki, D., Yamamoto, Y., 2010. A generalized method to estimate waveforms common across trials from EEGs. NeuroImage 51, 629–641.
Takeda, Y., Yamanaka, K., Yamagishi, N., Sato, M., 2014. Revealing time-unlocked brain activity from MEG measurements by common waveform estimation. PLoS One 9, e98014.
Tambini, A., Ketz, N., Davachi, L., 2010. Enhanced brain correlations during rest are related to memory for recent experiences. Neuron 65, 280–290.
Tong, Y., Hocke, L.M., Licata, S.C., Frederick, B., 2012. Low-frequency oscillations measured in the periphery with near-infrared spectroscopy are strongly correlated with blood oxygen level-dependent functional magnetic resonance imaging signals. J. Biomed. Opt. 17, 106004.
Tong, Y., Hocke, L.M., Fan, X., Janes, A.C., Frederick, B., 2015. Can apparent resting state connectivity arise from systemic fluctuations? Front. Hum. Neurosci. 9, 285.
Van de Ville, D., Britz, J., Michel, C.M., 2010. EEG microstate sequences in healthy humans at rest reveal scale-free dynamics. Proc. Natl. Acad. Sci. U. S. A. 107, 18179–18184.
Wilson, M.A., McNaughton, B.L., 1994. Reactivation of hippocampal ensemble memories during sleep. Science 265, 676–679.
Woolrich, M.W., Baker, A., Luckhoo, H., Mohseni, H., Barnes, G., Brookes, M., Rezek, I., 2013. Dynamic state allocation for MEG source reconstruction. NeuroImage 77, 77–92.

Supplementary Material

Estimating repetitive spatiotemporal patterns from resting-state brain activity data

Yusuke Takeda, Nobuo Hiroe, Okito Yamashita, Masa-aki Sato

Independent component analysis (ICA) and seed-based correlation analysis were applied to the preprocessed resting-state fMRI data to which the proposed method (STeP) was applied. In applying ICA, the data at each voxel was regarded as a sample, and the number of ICs was set to 20.

As a result, spatial patterns consistent with the default mode network were extracted. This suggests that the fMRI data were preprocessed properly.

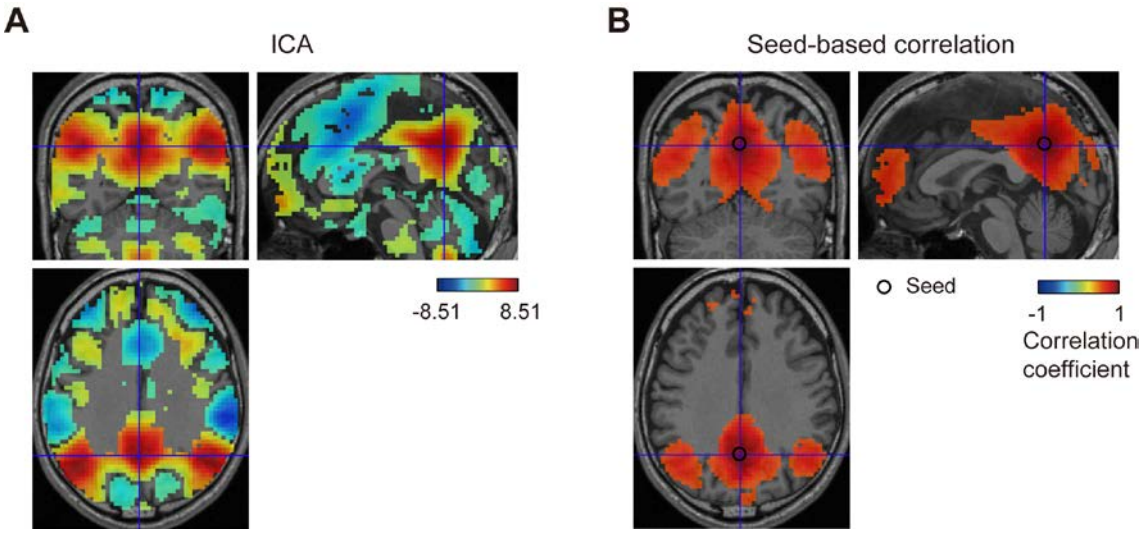

(A) Result of ICA. IC 5 is shown. Activities whose absolute values are over 0.1 of maximum value across voxels are shown. (B) Result of seed-based correlation analysis. Correlation coefficients whose absolute values are over 0.6 are shown.